GeoVirtual 2020 September 14-16
Resilience and Innovation

Seismic responses of monopile in sands under scour conditions

Wenyu Jiang, Cheng Lin
Department of Civil Engineering – University of Victoria, Victoria, BC, Canada

ABSTRACT
Monopile-supported offshore wind turbines (OWTs) are vulnerable to both scour and earthquake in seismically active regions. Scouring changes both dynamic characteristics and seismic demands of monopile. In general practice, an estimated maximum scour depth is used for the design of marine foundations. Nevertheless, the highest seismic demand for the monopile may not be associated with the maximum scour depth. Such combined effects of scour and earthquake on monopile responses are not well understood, particularly for live-bed conditions involving changeable scour depths. This study aims to fill this gap by conducting nonlinear time-domain dynamic analyses considering various scour depths. Through 30 parametric analyses, scour effects on seismic responses of monopiles in dense sands were investigated, and recommendations for selecting proper scour depths were made for the seismic design of monopile.

RÉSUMÉ
Les éoliennes offshores à monopile (OWT) sont vulnérables à la fois à l'affouillement et aux tremblements de terre dans les régions sismiquement actives. L'affouillement modifie à la fois les caractéristiques dynamiques et les exigences sismiques du monopile. En pratique générale, une profondeur d'affouillement maximale estimée est adoptée pour la conception des fondations des structures maritimes. Néanmoins, l'exigence sismique la plus élevée pour le monopile peut ne pas être associée à la profondeur d'affouillement maximale. Ces effets combinés de l'affouillement et du tremblement de terre sur les réponses des monopiles ne sont pas bien compris, en particulier pour les conditions de lit vivant impliquant des profondeurs d'affouillement variables. Cette étude vise à combler cette lacune en conduisant des analyses dynamiques non linéaires dans le domaine temporel en considérant différentes profondeurs d'affouillement. Grâce à 30 analyses paramétriques, les effets de l'affouillement sur les réponses sismiques des monopiles dans les sables denses ont été étudiés, et des recommandations pour la sélection des profondeurs d'affouillement appropriées ont été faites pour la conception sismique du monopile.

1 INTRODUCTION

The number of offshore wind farms has been increasing globally, due to the increasing demand for sustainable energies. In 2019, 39% and 59% of new offshore wind farms were installed in China and Europe, respectively, and offshore wind energy firstly reached a market share of 10% level in global new installations (GWEC 2020). Due to the ease of fabrication, installation, and operation, the monopile-supported offshore wind turbine (OWT) is a dominant type of OWT globally. A monopile is a tubular steel pile with an outside diameter of 4 to 6 m for supporting a tower and rotor-nacelle assembly (RNA) in water depths up to 35 m (Doherty and Gavin 2012).

Monopile-supported OWTs are often designed against cyclic loads due to rotor rotation, waves, and winds. Influenced by waves and currents, monopiles are also vulnerable to scour. In the seismically active zones such as the Pacific Northwest and East Asia, the damage to the OWT system can be magnified by the combined effects of scour and earthquake. Scour not only reduces monopile capacities but also changes the dynamic characteristics of the OWT system. Therefore, it is important to evaluate the scour effects on the seismic responses of the monopile-supported OWT.

The design of monopile-supported OWTs typically follows a "soft-stiff" rule such that the fundamental frequency falls within the range of rotor frequency and the range of blade-passing frequency to avoid resonance. However, scour may shift the fundamental frequency into the rotor frequency band and cause damages to both the wind turbine and supporting structure. For the live-bed scour condition, periodic changes in the dynamic characteristics of an OWT system may reduce its fatigue life and serviceability over a typical lifetime of 20–25 years (Carter 2007). Scour around a monopile includes both general scour (erosion across the seabed) and local scour (development of a hole around the pile); In routine design, when the scour dimensions are unavailable, the local scour

depth (current-induced) is often taken as 1.3D or 1.5D (D is the outside diameter of the monopile), and the effect of local scour on the soil resistance to the pile can be considered using the influence depth method (API 2011, DNV 2014). Alternatively, a simplified scour condition is usually assumed and adopted (Prendergast et al. 2015, Abhinav and Saha 2017, Li et al. 2018) with a total scour depth (i.e., general scour depth plus local scour depth) being 2.5D (GL 2012). The up-to-date maximum depth of a local scour observed at windfarms is 1.47D (Whitehouse et al. 2011), while it is still unclear whether these design values can provide a reliable prediction in the scour depth as limited data from field investigations (Matutano et al. 2013). At present, most studies (Prendergast et al. 2015, Abhinav and Saha 2017, Li et al. 2018) focus on the dynamic properties of OWTs such as the scour-induced shifts in the natural frequencies, while limited study (Jia et al. 2017) focuses on the seismic responses of OWTs under scoured conditions. Tempel et al. (2004) found that the increase in scour depth from 0 to 2.5*D* could decrease the fundamental frequency of the integrated OWT system by 6% and decrease the fatigue life by a factor of 4.3 for a 2.75 MW OWT in sands at a site off the Dutch coast. Moreover, the reduction in the fundamental frequency was found to be 8% at a scour depth of 1.5*D* for a 5 MW OWT in loose sands, which could shift the fundamental frequency into the rotor frequency band and cause resonance (Abhinav and Saha 2017). The above literature review indicates that more studies will be needed to improve the understanding of the post-scour seismic responses of the monopile-supported OWTs.

This study aimed to develop an open-source finite element model following the dynamic-beam-on-nonlinear-Winkler-foundation (DBNWF) approach for analyzing the dynamic responses of the monopile-supported OWTs in sands under general scour conditions. Using the validated computer script, a total number of 30 time-domain nonlinear analyses were performed considering six crustal earthquake motions and five general scour depths. Through the parametric analyses, the effects of scour depth on the natural frequencies of the integrated OWT system and the seismic responses of the monopile in dense sands were illuminated, and some design-related issues were also discussed.

2 OVERVIEW OF DESIGN METHODS FOR MONOPILE UNDER SCOURED CONDITION

This section summarizes current design considerations for the monopile-supported OWTs under the combined effects of scour and earthquake. Generally, there are three methods for analyzing the post-scour responses of the monopile-supported OWTs, including advanced continuum method (3D finite element or finite difference method), macro-element method (soil-pile interactions are represented by foundation spring-dashpot elements), and dynamic-beam-on-nonlinear-Winkler-foundation (DBNWF) method (Boulanger et al. 1999) (soil-pile interactions are modelled using p-y, t-z, and q-z springs in parallel with dashpots). Hitherto the DBNWF method is extensively used in routine design (Yang et al. 2019). Besides, compared with the macro-element method, the DBNWF method could provide reasonably accurate estimations of the natural frequencies (Tseng et al. 2018).

2.1 Scour consideration

Scour at a monopile usually consists of general scour and local scour. Thereinto, the local scour hole is commonly idealized as a truncated cone with a side slope angle of 30° and a depth of 1.3D (DNV 2014) or 1.5D (API 2011), and several standard methods (Patrick et al. 2016) recommend modifying the conventional p-y curves via the influence depths to account for the three-dimensional scour holes with the prescribed dimensions. Thereinto, compared with the scour bottom width and side slope angle, the scour depth is generally a dominant factor that determines the pile responses (Lin and Lin 2019). However, the local scour hole is often simplified as a general scour (termed as simplified scour condition) in routine design and recent studies (Prendergast et al. 2015, Abhinav and Saha 2017, Li et al. 2018), for which an estimated maximum scour depth of 2.5D (GL 2012) is typically adopted. Although this simplification could cause 49%–68% higher groundline lateral displacements of single piles in sands under a typical range of static lateral loads (Lin et al. 2014), considering the scour depth is the most important factor among the scour-hole dimensions and the focus of this study is the scour-induced variations (rather than specific evaluations) in the seismic responses of monopiles, the simplified scour condition is adopted herein to be consistent with the routine design, while the more realistic local scour condition will be investigated in the future studies.

2.2 Seismic consideration

At present, there are four design guidelines (Risø 2002, IEC 2005, GL 2012, DNV 2014) that specify the seismic design of OWTs, while they are generally less detailed than the building codes. OWTs are typically designed against the earthquake with a 475-year return period. Although both the frequency-domain method and time-domain method are specified by these guidelines, the time-domain solution is preferable as the frequency-domain method could underestimate the design demand (Yang et al. 2019). Moreover, instead of uniformly exciting an entire OWT system using the recorded acceleration time history, the depth-specific seismic inputs from the free-field analysis shall be used to avoid underestimating the structural responses (Kim et al. 2014). In general, seismic responses of a monopile are governed by the top layer of a deposit (Li et al. 2018). Based on the foregoing summary, the time-domain DBNWF approach is adopted in this study to evaluate the post-scour responses of the monopile-supported OWTs, in which the general scour is simulated by removing the soil springs within the scour depth.

3 PROPOSED MODEL

To evaluate the monopile seismic responses, an integrated OWT model including the soil, monopile, and structure was

established instead of a simple soil-pile model. This integrated model allows for more accurate evaluations of the monopile seismic responses as the incorporation of both inertial and kinematic effects. Figure 1(a) illustrates a monopile-supported OWT in the sand under the combined effects of earthquake and general scour. Figure 1(b) illustrates the finite element model developed in an open-source platform OpenSees (McKenna 2011), where the rotor-nacelle assembly (RNA) was simplified as a lumped mass atop the tower according to Arany et al. (2017). The tubular tower and monopile were modelled as the nonlinear displacement-based beam elements with three-dimensional fibre sections. Three translational degrees of freedom (DOFs) and three rotational DOFs were designated to the beam-element nodes. The second-order P-delta effect was considered since the OWT is a laterally loaded structure with a heavy RNA on its top.

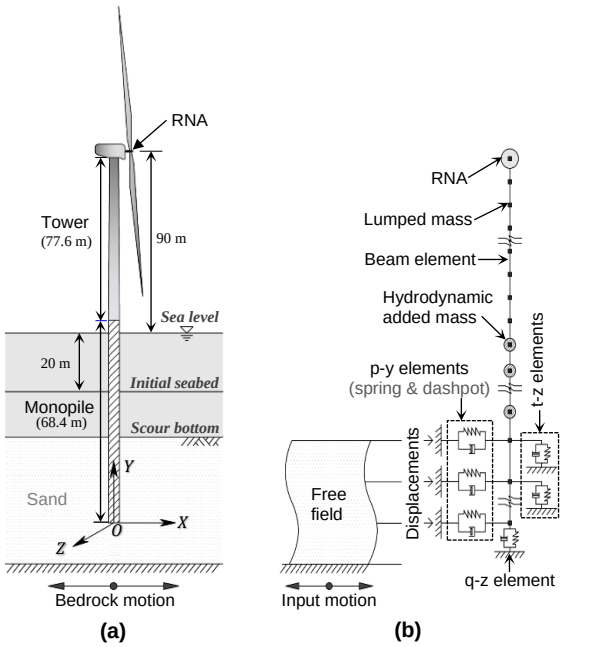

Figure 1. Illustrations of (a) physical model and (b) numerical model for a monopile-supported OWT under combined effects of scour and earthquake

Furthermore, the energy dissipation of the OWT system under an earthquake excitation was simulated by Rayleigh damping. A parked state of the wind turbine was considered here to exclusively investigate the seismic behaviour, thus the total damping ratio of the integrated system consisted of hydrodynamic damping ratio (0.37%) and hysteresis damping ratios of structure (0.3%) and soil (5%) (GL 2012, DNV 2014).

3.1 Monopile-soil interaction under scour condition

The monopile-soil interactions in sands were simulated using the API (2011) p-y, t-z, and q-z springs in parallel with dashpots. The dashpots were used for considering the energy dissipations for the high-frequency vibrations caused by earthquakes. Under the simplified scour condition, the spring-dashpot elements within the scour depth were simply removed, and the remaining spring-dashpot elements below the post-scour seabed were evaluated using the conventional methods but with the post-scour soil depths.

3.1.1 Vertical springs and dashpots

The vertical springs around a monopile consisted of t-z and q-z springs with the load-displacement curves primarily dependent on the ultimate soil resistance.

$$t_{\mathrm{u}} = \beta \gamma' z \quad [1]$$

$$q_{\mathrm{u}} = N_{\mathrm{q}} \gamma' L_{\mathrm{e,sc}} \quad [2]$$

where t_{u} and q_{u} are the ultimate resistance of t-z and q-z spring, respectively; β and N_{q} are the friction factor and end bearing factor, respectively, dependent on the relative density of soil; γ' is the buoyant unit weight of soil; z is the soil depth below the post-scour seabed; and $L_{\mathrm{e,sc}}$ is the post-scour pile embedded length. Moreover, the viscous dashpot coefficient (Berger et al. 1977) was calculated from

$$c_{\mathrm{v}} = \Delta z \left[2\pi D \sqrt{(\gamma'/g + \rho_{\mathrm{s}}) G_{\max}} \right] \quad [3]$$

where Δz is the pile element size; D is the pile outside diameter; ρ_{w} is the mass density of water; and $G_{\max}$ is the small-strain shear modulus of soil.

3.1.2 Lateral springs and dashpots

The API (2011) sand p-y curve is mainly dependent on the ultimate lateral resistance, p_{u}, and initial modulus of subgrade reaction, k.

$$p = A p_{\mathrm{u}} \tanh \left[\frac{kzy}{(A p_{\mathrm{u}})} \right] \quad [4]$$

$$p_{\mathrm{u}} = \min[(C_1 z + C_2 D)\gamma' z, C_3 D \gamma' z] \quad [5]$$

where p is the lateral soil resistance; y is the lateral pile displacement; A is the load-type factor (taken as 0.9 here). The three constants ($C_1 - C_3$) and k are determined based on the internal friction angle of soil. Moreover, the radiation damping coefficient for the horizontal viscous dashpot (Berger et al. 1977) was evaluated as

$$c_{\mathrm{h}} = \Delta z \left[4D \sqrt{(\gamma'/g + \rho_{\mathrm{w}}) G_{\max}} \right] \quad [6]$$

3.2 Monopile-water interaction under scour condition

The monopile-water interaction was simulated by the added mass distributed on the submerged monopile in the conventional dynamic analysis (Goyal and Chopra 1989). The outside and inside added mass functions above the post-scour seabed for a unit length of pile, $m_{\mathrm{a}}^{\mathrm{o}}(h_{\mathrm{s}})$ and $m_{\mathrm{a}}^{\mathrm{i}}(h_{\mathrm{s}})$, are given by

$$m_{\mathrm{a}}^{\mathrm{o}}(h_{\mathrm{s}}) = \frac{16\rho_{\mathrm{w}}h_{\mathrm{o}}}{\pi}\left[\sum_{m=1}^{\infty}\frac{(-1)^{m-1}K_1\alpha_m r_{\mathrm{po}}\cos(\alpha_m h_{\mathrm{s}}/h_{\mathrm{o}})}{(2m-1)^2(K_0+K_2)\alpha_m}\right] \quad [7]$$

$$m_{\mathrm{a}}^{\mathrm{i}}(h_{\mathrm{s}}) = \frac{16\rho_{\mathrm{w}}h_{\mathrm{i}}}{\pi}\left[\sum_{m=1}^{\infty}\frac{(-1)^{m-1}I_1\alpha_m r_{\mathrm{ip}}\cos(\alpha_m h_{\mathrm{s}}/h_{\mathrm{i}})}{(2m-1)^2(I_0+I_2)\alpha_m}\right] \quad [8]$$

where I_n is the modified Bessel function of order n of the first kind; K_n is the modified Bessel function of order n of the second kind; h_{s} is the distance from a pile node of interest to the post-scour seabed; h_{o} and h_{i} are the water depths outside and inside the monopile, respectively; r_{op} and r_{ip} are the outside and inside radius of the monopile, respectively; $\alpha_m = (2m-1)\pi/2$ with m being an integer.

3.3 Earthquake loading

The seismic excitation was achieved by applying the free-field displacements to the ends of the spring-dashpot elements, and the free-field displacements were calculated from the equivalent nonlinear site response analysis (SRA) in DEEPSOIL with the input of the recorded earthquake motions. The input earthquake motions will be discussed in the next section. The soil profile for the SRA was developed from the post-scour seabed to the bedrock (or firm ground), and the soil nonlinearities were represented by the modulus reduction curve and damping ratio curve proposed by Darendeli (2001). Besides, the unit weight and shear wave velocity of the firm ground were taken as 21.58 kN/m^3 and 760 m/s, respectively. Furthermore, the free-field accelerations were processed using a signal processing script in MATLAB and then integrated to generate the free-field displacements.

3.4 Validation for script

The DBNWF method for the seismic analyses has been extensively validated by comparing the results with the centrifuge test data (Wang et al. 1998, Boulanger et al. 1999) and with the results from sophisticated finite element models (Kampitsis et al. 2013). Besides, this method has been widely used for the analyses of monopile-supported OWTs (Jonkman and Musial 2010, DNV 2014, Yang et al. 2019). Therefore, the DBNWF method can be confidently used for the analysis of monopile-supported OWTs under the combined effects of general scour and earthquake.

Here, we were to validate the developed script for the DBNWF model. A published pre-scour case (Yang et al. 2019) involving the eigenvalues for a seismically loaded monopile-supported OWT in layered sands was referenced to verify the correctness of the script. The fundamental frequency computed using the developed script was 0.30 Hz, which agreeably matches with the published value (0.25 Hz). This discrepancy is acceptable as in the model the RNA was a lumped mass and soil deposit was a single layer with thickness-averaged soil parameters but Yang et al. (2019) explicitly modelled the RNA and layered soil deposit. Overall, credence is given to the proposed model.

4 PARAMETRIC ANALYSES

The US National Renewable Energy Laboratory 5 MW baseline wind turbine (Jonkman et al. 2019) was selected as the case study, the corresponding parameters of the structural components are listed in Table 1.

Table 1. Parameters of structural components

Monopile (Nonlinearity)	Length (m)	68.4
	Embedded length (m)	36
	Outside diameter (m)	6
	Wall thickness (m)	0.06
	Poisson's ratio	0.3
	Elastic modulus (GPa)	210
	Yield strength (GPa)	0.408
	Mass density (kg/m^3)	8500
Tower* (Nonlinearity)	Height (m)	77.6
	Outside diameter (m)	3.876–6.0
	Wall thickness (m)	0.019–0.027
RNA	Height above sea level (m)	90
	Mass (ton)	350

*Note: tower and monopile have identical material properties

Table 2 lists the six ground motions corresponding to different crustal earthquakes used for the seismic analyses. These time series were scaled to the same peak ground accelerations (PGAs) of 0.5g and used as the bedrock input motions for the SRA. Besides, the calculated 5% damped response spectra for a single-degree-of-freedom structure are shown in Figure 2.

Table 2. Information about bedrock input motions

Earthquake event	M_{w}	Type[1]	RSN/Comp.[2]	$D_{a5\text{-}95}$ (s)[3]
Chalfant Valley, 1986	6.19	SS	549/180	12.55
Loma Prieta, 1989	6.93	RO	769/000	12.96
Northridge, 1994	6.69	R	1011/185	6.66
Kobe, 1995	6.90	SS	1111/000	9.59
Chi-Chi, 1999	7.62	RO	1521/000	24.11
Kocaeli, 1999	7.51	SS	1158/180	11.79

[1]Fault type: SS=strike slip, RO=reverse oblique, R=reverse

[2]RSN=record sequence number, Comp.=component

[3]Significant duration (i.e., the time interval between the points at which 5% and 95% of the total energy has been recorded)

The soil considered herein was dense sand from a test site for laterally loaded single piles (Cox et al. 1974). The soil properties included the relative density (D_r=90%), buoyant unit weight (γ'=10.4 kg/m^3), and internal friction angle (ϕ'=38.8°). The small-strain shear moduli, G_{max}, of the soil deposit were between 33 kPa and 254 kPa, calculated according to Seed et al. (1986). Correspondingly, the fundamental period of the OWT system before scour was 3.3 s. A closer examination of Figure 2 indicates the six spectral accelerations exhibited some variations, particularly in the large periods, and they generally decreased with the increase in the range of period of interest for the OWT ($0.15T_a$–$2.0T_a$, where T_a is the fundamental period of the integrated OWT system). The use of the time-domain scaling rather than the spectral matching was to reveal the inherent variabilities of different earthquake motions. Therefore, it is anticipated that the seismic responses corresponding to these six ground motions would exhibit certain variations besides some general trends. Meanwhile, five general scour depths ranging from $0.5D$ to $3.5D$ were examined for each earthquake motion to evaluate the scour effects. Correspondingly, a total of 30 dynamic cases were analyzed. It should be noted that these investigated scour depths were selected based on the typical design values ($1.3D$–$2.5D$) (API 2011, GL 2012, DNV 2014) and field investigation data (Whitehouse et al. 2011).

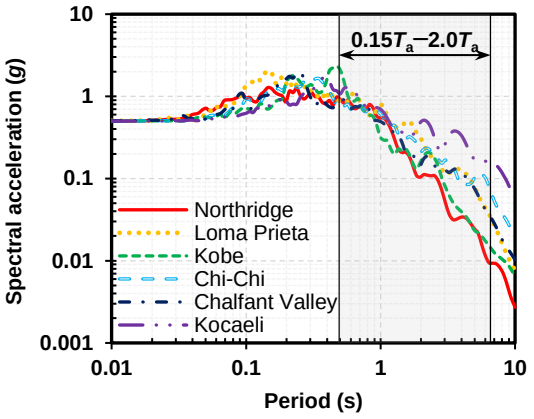

Figure 2. Response spectra of input acceleration records

5 RESULTS AND DISCUSSION

The effects of scour depth on the natural frequencies of the integrated OWT system, the maximum bending moment of the monopile, and the maximum rotation of the monopile at the post-scour seabed are presented subsequently.

5.1 Effects of scour depth on frequency

Based on the design criterion of the serviceability limit state, the fundamental frequency of the integrated OWT system should be offset from the frequencies of rotor rotation (f_{1P}) and blade passing (f_{3P} for a three-blade turbine) by at least 10% to avoid resonance (DNV 2014). Figure 3 is the Campbell diagram for the integrated OWT system investigated in the paper under different general scour depths. As shown, the pre-scour integrated system fell in a "soft-stiff" zone in the operation range of the wind turbine (i.e., between the cut-in speed and cut-out speed). However, the fundamental frequency decreased by 10%–20% when $S_d = 1.3D$–$2.5D$, and it fell into the range of f_{1P} when $S_d > 1.3D$, violating the serviceability criterion.

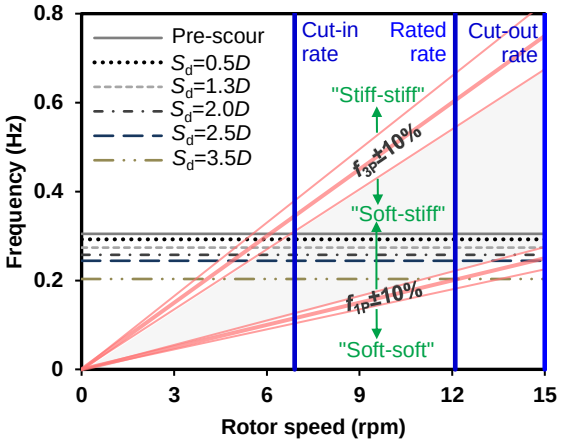

Figure 3. Fundamental frequencies of the integrated OWT system varied with scour depths

Moreover, Figure 4 shows the effects of scour depth on the normalized natural frequencies of the integrated OWT system, where the natural frequencies were normalized by the fundamental frequency of the soil deposit.

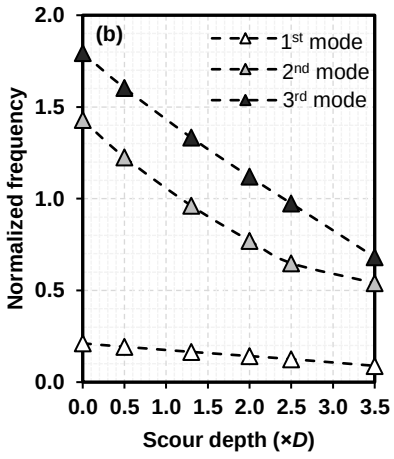

Figure 4. Normalized natural frequencies varied with scour depths

As shown in Figure 4, the normalized frequencies corresponding to the second and third eigenmodes were approximately equal to 1.0 when $S_d = 1.3D$–$2.5D$, which

indicates that the higher-mode contributions were considerable for the dynamic responses of the OWT system. As will be discussed later, certain seismic responses of the monopile appeared to reach the peaks when $S_d = 1.3D$–$2.5D$. Therefore, it is necessary to select a proper range of scour depths in design to capture the peak seismic responses.

5.2 Effects of scour depth on maximum responses of monopile

The maximum dynamic responses of the monopile under different scour depths are presented in normalized forms by comparing them to the pre-scour responses using the following three steps:

(1) Determine the maximum time-domain responses at different locations on the monopile and plot them as the response envelopes (e.g., Figure 5).
(2) Determine the maximum responses of the monopile at the post-scour seabed level and the maximum responses of the monopile from the response envelopes.
(3) Determine the normalized response by dividing the post-scour maximum response by the corresponding pre-scour value, and thus a ratio greater than one indicates the amplification of the seismic response and vice versa.

5.2.1. Maximum bending moment of monopile

To demonstrate the above procedure, Figure 5 profiles the bending moment envelopes of the monopile before and after scour ($S_d = 1.3D$) under the input motion corresponding to the Loma Prieta earthquake. From the figure, increasing S_d from 0 to $1.3D$ increased the maximum bending moment by 8%, and the corresponding normalized maximum bending moment was 1.08. Besides, the location corresponding to the maximum bending moment was $2.0D$ below the post-scour seabed. Likewise, the normalized maximum bending moments of the monopile under different scour depths and other earthquakes were determined and plotted in Figure 6.

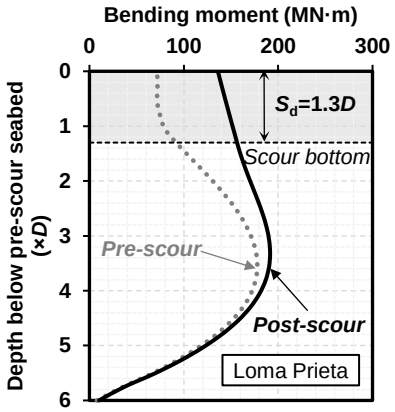

Figure 5. Envelopes of monopile bending moment before and after scour ($S_d = 1.3D$)

Figure 6 shows a relatively scatter distribution of the normalized maximum bending moments. However, the trendline (based on the second-order regression) indicates that the maximum bending moment was amplified due to scour when $S_d = 0.5D$–$2.5D$ and the peak amplification on average reached 15% when $S_d = 1.3D$–$2.0D$. Contrarily, the maximum bending moment averagely decreased by 20% when $S_d = 3.5D$.

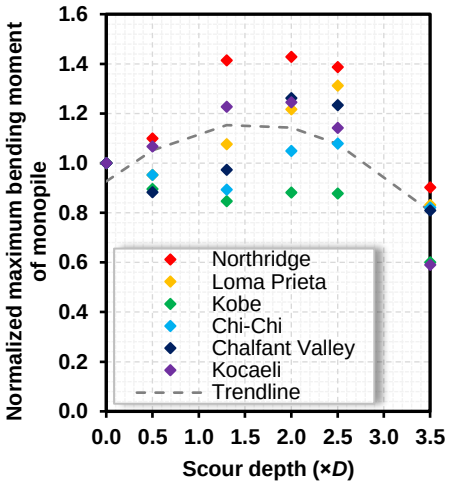

Figure 6. Normalized maximum bending moments of monopile under different scour depths

5.2.2. Maximum rotation of monopile

Figure 7 profiles the monopile rotations before and after scour ($S_d = 1.3D$) under the Loma Prieta earthquake. The post-scour pile rotations increased averagely by 73% when $S_d = 1.3D$ compared with the pre-scour rotations as the reduced lateral stiffness of the monopile.

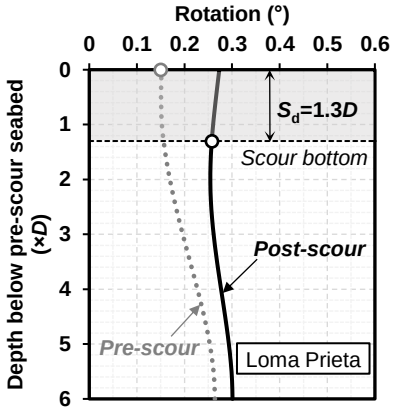

Figure 7. Envelopes of monopile rotation before and after scour ($S_d = 1.3D$)

Furthermore, most design practices specify the rotation requirement at the seabed level. Therefore, the normalized maximum rotation was defined as a ratio of the post-scour rotation of the monopile at the post-scour seabed to the pre-scour rotation of the monopile at the pre-scour seabed (see the circles in Figure 7). The normalized maximum rotation in Figure 7 is 1.67. Adopting the above procedure, the normalized maximum rotations of the monopile at the post-scour seabed were determined for different scour depths and plotted in Figure 8, where the trendline was obtained based on the second-order regression.

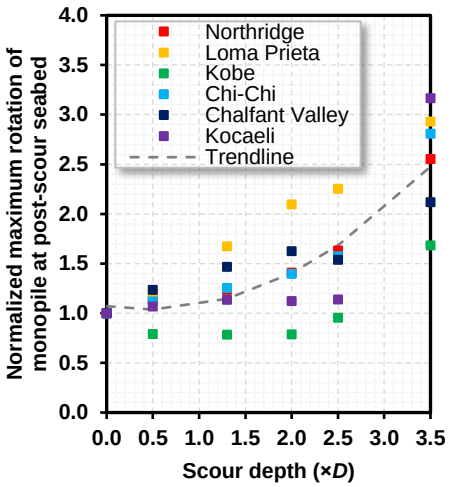

Figure 8. Normalized maximum rotations of monopile at post-scour seabed under different scour depths

As shown in Figure 8, the maximum rotations in general increased by 14%–68% when $S_d = 1.3D$–$2.5D$ since the lateral stiffness of the monopile-soil system kept decreasing with the increased scour depth. The serviceability criterion based on DNV (2014) requires that the accumulated monopile rotation at the seabed level should be less than 0.5° and the calculated rotations were within this limit. Therefore, the use of greater value within the typical scour depth range ($1.3D$–$2.5D$) is recommended as it provided conservative estimation for the monopile rotation.

6 CONCLUSIONS

This study investigated the monopile responses under the combined effects of scour and earthquake by conducting 30 nonlinear time-domain seismic analyses of the integrated OWT model. The results included the natural frequencies of the integrated OWT system, maximum bending moments of the monopile, and maximum rotations of the monopile at the post-scour seabed. Based on the results of the analyses, the following conclusions were obtained:

(1) The fundamental frequency of the integrated soil-monopile-tower-turbine system could decrease to the range of rotor frequency, causing resonance when $S_d > 1.3D$.

(2) An increase in scour depth caused mixed increase and decrease in the maximum bending moment of the monopile, but a consistent increase in the maximum rotation of the monopile at the post-scour seabed.

(3) For the maximum bending moment of the monopile, there exists a range of critical scour depths, i.e., $1.3D$–$2.0D$. This critical scour depth range is recommended for evaluating the maximum bending moments. The use of an excessive scour depth (i.e., $S_d > 2.0D$) could underestimate the maximum bending moment of the monopile by up to 20%.

(4) For the maximum rotation of the monopile at the post-scour seabed, a large scour depth needs to be used. For the design practices that employ the scour depth of $1.3D$–$2.5D$, a scour depth of $2.5D$ is recommended for evaluating the maximum rotation.

ACKNOWLEDGEMENTS

The authors would like to acknowledge the Natural Sciences and Engineering Research Council of Canada (NSERC) for supporting this study through the NSERC Discovery Grant.

REFERENCES

Abhinav, K.A., and Saha, N. 2017. Effect of Scouring in Sand on Monopile-supported Offshore Wind Turbines, *Marine Georesources and Geotechnology*, 35(6): 817–828.

American Petroleum Institute (API). 2011. *API RP 2GEO: Recommended Practice, Geotechnical and Foundation Design Considerations*, American Petroleum Institute (API), Washington, D.C., USA.

Arany, L., Bhattacharya, S., Macdonald, J., and Hogan, S.J. 2017. Design of Monopiles for Offshore Wind Turbines in 10 Steps, *Soil Dynamics and Earthquake Engineering*, 92: 126–152.

Berger, E., Mahi, S.A., and Pyke, R. 1977. Simplified Method for Evaluating Soil-pile-structure Interaction Effects, *The 9th Annual Offshore Technology Conference*, Offshore Technology Conference, Houston, Texas, USA, 589-598.

Boulanger, R.W., Curras, C.J., Kutter, B.L., Wilson, D.W., and Abghari, A. 1999. Seismic Soil-pile-structure Interaction Experiments and Analyses, *Journal of Geotechnical and Geoenvironmental Engineering*, American Society of Civil Engineers (ASCE), 125(9): 750–759.

Carter, J.M.F. 2007. North Hoyle Offshore Wind Farm: Design and Build, *Proceedings of the Institution of Civil Engineers (ICE) - Energy*, ICE Publishing, 160(1): 21–29.

Cox, W.R., Reese, L.C., and Grubbs, B.R. 1974. Field Testing of Laterally Loaded Piles in Sand, *The 6th*

Annual Offshore Technology Conference, Offshore Technology Conference, Houston, Texas, USA, 459-473.

Darendeli, M.B. 2001. *Development of a New Family of Normalized Modulus Reduction and Material Damping Curves*, PhD thesis, The University of Texas, Austin, Texas, USA.

Det Norske Veritas (DNV). 2014. *Design of Offshore Wind Turbine Structures*, Det Norske Veritas (DNV), Oslo, Norway.

Doherty, P., and Gavin, K. 2012. Laterally Loaded Monopile Design for Offshore Wind Farms, *Proceedings of the Institution of Civil Engineers - Energy*, ICE Publishing, 165(1): 7–17.

Germanischer Lloyd (GL). 2012. *Guideline for the Certification of Offshore Wind Turbines*, Germanischer Lloyd (GL) Renewables Certification, Hamburg, Germany.

Global Wind Energy Council (GWEC). 2020. *Global Wind Report 2019*, Global Wind Energy Council (GWEC), Brussels, Belgium.

Goyal, A., and Chopra, A.K. 1989. Simplified Evaluation of Added Hydrodynamic Mass for Intake Towers, *Journal of Engineering Mechanics*, American Society of Civil Engineers (ASCE), 115(7): 1393–1412.

International Electrotechnical Commission (IEC). 2005. *Wind Turbines - Part 1: Design Requirements (3rd Edition)*, International Electrotechnical Commission (IEC), Geneva, Switzerland.

Jia, N., Ding, H., Zhang, P., and Liu, J. 2017. The Seismic Response of Composite Bucket Foundation for Offshore Wind Turbines under Scour Conditions, *The 27th International Ocean and Polar Engineering Conference*, International Society of Offshore and Polar Engineers (ISOPE), San Francisco, CA, USA, 344-350.

Jonkman, J., Butterfield, S., Musial, W., and Scott, G. 2019. *Definition of a 5-MW Reference Wind Turbine for Offshore System Development*, National Renewable Energy Laboratory (NREL), Golden, Colorado, USA.

Jonkman, J., and Musial, W. 2010. *Offshore Code Comparison Collaboration (OC3) for IEA Task 23 Offshore Wind Technology and Deployment*, National Renewable Energy Laboratory (NREL), Golden, Colorado, USA.

Kampitsis, A.E., Sapountzakis, E.J., Giannakos, S.K., and Gerolymos, N.A. 2013. Seismic Soil-pile-structure Kinematic and Inertial Interaction–a New Beam Approach, *Soil Dynamics and Earthquake Engineering*, 55: 211–224.

Kim, D.H., Lee, S.G., and Lee, I.K. 2014. Seismic Fragility Analysis of 5 MW Offshore Wind Turbine, *Renewable Energy*, 65: 250–256.

Li, H., Ong, M.C., Leira, B.J., and Myrhaug, D. 2018. Effects of Soil Profile Variation and Scour on Structural Response of an Offshore Monopile Wind Turbine, *Journal of Offshore Mechanics and Arctic Engineering*, American Society of Mechanical Engineers (ASME) Digital Collection, 140(4).

Lin, C., Han, J., Bennett, C., and L. Robert, P. 2014. Behavior of Laterally Loaded Piles under Scour Conditions Considering the Stress History of Undrained Soft Clay, *Journal of Geotechnical and Geoenvironmental Engineering*, American Society of Civil Engineers (ASCE), 140(6): 06014005.

Lin, Y., and Lin, C. 2019. Effects of Scour-hole Dimensions on Lateral Behavior of Piles in Sands, *Computers and Geotechnics*, 111: 30–41.

Matutano, C., Negro, V., López-Gutiérrez, J.-S., and Esteban, M.D. 2013. Scour Prediction and Scour Protections in Offshore Wind Farms, *Renewable Energy*, 57: 358–365.

McKenna, F. 2011. OpenSees: A Framework for Earthquake Engineering Simulation, *Computing in Science Engineering*, 13(4): 58–66.

Patrick, J.H., Frank, R., Garland, E.L., Brent, R.R., and Matthew, L.B. 2016. *Design and Construction of Driven Pile Foundations*, Federal Highway Administration, U.S. Department of Transportation, Washington, D.C., USA.

Prendergast, L.J., Gavin, K., and Doherty, P. 2015. An Investigation into the Effect of Scour on the Natural Frequency of an Offshore Wind Turbine, *Ocean Engineering*, 101(0): 1–11.

Risø. 2002. *Guidelines for Design of Wind turbines (2nd Edition)*, Risø National Laboratory and Det Norske Veritas (DNV), Roskilde and Copenhagen, Denmark.

Seed, H.B., Wong, R.T., Idriss, I.M., and Tokimatsu, K. 1986. Moduli and Damping Factors for Dynamic Analyses of Cohesionless Soils, *Journal of Geotechnical Engineering*, American Society of Civil Engineers (ASCE), 112(11): 1016–1032.

Tempel, J. van der, Zaaijer, M.B., and Subroto, H. 2004. The Effects of Scour on the Design of Offshore Wind Turbines, *The 3rd International Conference on Marine Renewable Energy (MAREC 2004)*, The East of England Energy Group (EEEGR), Newcastle, UK.

Tseng, W.-C., Kuo, Y.-S., Lu, K.-C., Chen, J.-W., Chung, C.-F., and Chen, R.-C. 2018. Effect of Scour on the Natural Frequency Responses of the Meteorological Mast in the Taiwan Strait, *Energies*, 11(4): 823.

Wang, S., Kutter, B.L., Chacko, M.J., Wilson, D.W., Boulanger, R.W., and Abghari, A. 1998. Nonlinear Seismic Soil-pile Structure Interaction, *Earthquake Spectra*, 14(2): 377–396.

Whitehouse, R.J.S., Harris, J.M., Sutherland, J., and Rees, J. 2011. The Nature of Scour Development and Scour Protection at Offshore Windfarm Foundations, *Marine Pollution Bulletin*, 62(1): 73–88.

Yang, Y., Bashir, M., Li, C., and Wang, J. 2019. Analysis of Seismic Behaviour of an Offshore Wind Turbine with a Flexible Foundation, *Ocean Engineering*, 178: 215–228.